Smart Materials and Structures

4D printed shape memory sandwich structures: Experimental analysis and numerical modeling

To cite this article before publication: Ahmad Serjouei *et al* 2022 *Smart Mater. Struct.* in press https://doi.org/10.1088/1361-665X/ac60b5

4D printed shape memory sandwich structures: Experimental analysis and numerical modeling

A. Serjouei[1], A. Yousefi[1], A. Jenaki[2], M.Bodaghi[1], M. Mehrpouya[2,3*]

[1] Department of Engineering, School of Science and Technology, Nottingham Trent University, Nottingham NG11 8NS, UK

[2] Department of Industrial Engineering and Management, HZ University of Applied Science, Het Groene Woud 1-3, 4331, NB Middelburg, The Netherlands

[3] Faculty of Engineering Technology, University of Twente, P.O. Box 217, 7500 AE Enschede, the Netherlands

Corresponding e-mail: m.mehrpouya@utwente.nl

Abstract

Additive manufacturing has provided a unique opportunity to fabricate highly complex structures as well as sandwich structures with various out-of-plane cores. The application of intelligent materials, such as shape memory polymers, gives an additional dimension to the three-dimensional (3D) printing process, known as four-dimensional (4D) printing, so that the deformed structures can return to their initial shape by the influence of an external stimulus like temperature. In this study, 4D printing of smart sandwich structures with the potential of energy absorption is investigated. The samples were fabricated considering various process parameters (i.e., layer height, nozzle temperature, printing velocity, and wall thickness) and tested mechanically. The experimental work reveals that the deformed sandwiches can fully recover their initial form by applying simple heating. Besides, a reliable finite element model (FEM) was developed to predict the functional behavior of the horseshoe sandwich structures in compression analysis. The experimental and simulation results show that among process parameters, wall thickness, layer height, and nozzle temperature are the most significant parameters to increase the compressive load and, consequently, the energy absorption rate. The concept, results, and modeling provided in this study are expected to be used in the design and fabrication of 4D printed sandwich structures for energy absorption applications.

Keywords: Additive manufacturing; 4D printing; Shape memory polymers; Sandwich structures; Auxetic; Energy absorption; Finite element modeling.

1-Introduction

The application of intelligent materials in additive manufacturing processes can provide a unique opportunity to design and fabricate smart three-dimensional (3D) printable products which are able to, e.g., alter their shape or volume [1, 2] when exposed to various stimuli; therefore, they are called 4D printed products [3]. Shape memory polymers (SMPs) are in the group of smart materials that can be programmed mechanically and have the characteristic of high-temperature shape recovery [4, 5]. Various 3D printing technologies can be applied for the fabrication of SMPs products, however, Fused Deposition Modeling (FDM) technology is a common printing method. This is mainly because both material and fabrication processes are inexpensive and it is easy-to-use technology. Also, they have low density and large deformability in the elastic field that makes them an ideal material for the 4D printing process [6-8].

There are three main steps in the 4D printing of SMPs. In the first step, they can be printed in a temporary form, then achieve a permanent deformation by applying an external force. The second step is called programming, and the deformed sample can retrieve the initial (permanent) form in the third step by applying temperature gradient as an external stimulus [9]. SMPs are mostly programmed by thermo-mechanical stimuli; however, they are sensitive to various stimuli such as temperature [10, 11], magnetic energy [12], moisture [13], etc. The application of 3D printing technology can open up great opportunities to fabricate geometrically complex structures such as sandwich panels with the potential of a stress absorber panel [14, 15]. According to various studies [16-18], the functional behavior and mechanical properties of the sandwich structures have a direct relation to the design and geometry of the cellular core such as origami-inspired structures [19-21], or bioinspired designs [22, 23]. For this purpose, additive manufacturing technologies are very beneficial in order to design and fabricate complex shape structures as well as metamaterial design with particular functionality [24, 25]. In particular, if there is a need for energy and vibration damping, the new studies show that the application of auxetic structures with a negative Poisson's ratio can effectively improve the resistance and vibration properties and also increase the energy absorption rate of the structures [26-30]. In recent years, these structures, well-known as meta-sandwich structures, have been widely used for energy absorption applications such as sports equipment, protective packaging, or automotive protection parts [31, 32]. They are able to absorb a high amount of stress level that makes them capable of converting kinetic energy to large elastic-plastic deformations [33-35].

There are various studies that can show the capability of 4D printed sandwich structures. For instance, *Mehrpouya et al.* [36] applied Polylactic acid (PLA) material in the 4D printing of honeycomb sandwich structure fabricated by FDM. They investigated the impact of printing parameters on the shape recovery ratio of the deformed structures. They reported that lower printing speed and higher nozzle and activation temperatures can enhance the shape recovery rate. *Bodaghi et al.* [37] also employed 4D printing to fabricate dual-material sandwich structures by FDM. They investigated the functionality and energy absorption rate in auxetic meta-sandwiches with the application of various materials and revealed the full recovery of the deformed structure by simple heating. *Barletta et al.* [38] used PLA in 4D printing of smart sandwich structures fabricated by FDM. They showed that operational parameters, particularly activation temperature, have a significant impact on the functionality and shape recovery rate of the deformed parts. In a similar study, *Zeng et al.* [39] designed horseshoe lattice structures with different sizes and angles. They reported the structural design has a direct impact on deformation behavior and finally the functionality of the 4D printed part. *Liu et al.* [40] also reported the 4D printing process of metamaterial spring with the potential of mechanical and vibration isolation. They designed and fabricated a cylindrical shape of an auxetic structure by FDM that effectively can reduce the vibration amplitude and have a good shock absorption performance.

In this paper, 4D printed sandwich structures are developed by FDM 4D printing technology for reversible energy absorption applications. The study investigates the effect of design and process parameters on the stress absorption rate and shape recovery behavior of 4D printed sandwich structures. For this purpose, two auxetic sandwich structures are designed with different inner cores and geometries. Then, all specimens are fabricated via an FDM 3D printer and tested by compression tests for evaluating the stress absorption rate. The shape memory behavior of samples is investigated by varying the deposition speed, the nozzle temperature of the extruder, and layer thickness as well. A finite element simulation is also established in order to predict the mechanical behaviors of the 4D printed energy absorbers during the loading and unloading process. It is observed that the elastic-plastic compressive behavior, energy absorption capacity, and shape recovery behavior of 4D printed sandwich structures can be modeled accurately by finite element modeling. Due to the absence of similar results in the specialized literature, this

paper is likely to fill a gap in the state of the art of this problem and provide pertinent results that are instrumental in 4D printing sandwich structures for energy absorption applications.

2-Materials and methods

2.1 Material

PLA Filament (*Ultimaker, the Netherlands*) with a diameter of 2.85 ± 0.10 mm was used in this study. Table 1 shows the thermo-mechanical properties of the material in more detail.

Table 1. Properties of PLA filament

Properties	Value	Regulation
Melting temperature	145 - 160 °C	ISO 11357
Glass transition temperature	~ 60 °C	ISO 11357
Izod impact strength notched (at 23 °C)	5.1 kJ/m2	ISO 180
Elongation at break	5.2%	ISO 527 (50 mm/min)
Tensile strength at break	45.6 MPa	ISO 527 (50 mm/min)
Flexure modulus	3,150 MPa	ISO 178
Melt mass-flow rate (MFR)	6.09 g/10 min	ISO 1133 (210 °C, 2.16 kg)

2.2 Design of sandwich structures

Among various shapes and geometries, two bio-inspired horseshoe-shaped structures with a negative Poisson's ratio are designed for this study. This is because of the capability of high deformation of these structures that enhances the energy absorption of the sandwich structures [41]. Figure 1 demonstrates the schematic of the CAD design of two models, including hexagonal and square horseshoe shapes. The structures contract laterally under a uniaxial compression force; in this way, the auxetic geometry has the energy absorption capability due to high shear strength. The design strategy for these models was to achieve the maximum compression ratio without material fracture. First, the CAD models are designed in *Solidworks (Dassault Systèmes, USA)*, further transformed into '.gcode' using the *Cura 4.7 (Ultimaker, The Netherlands)* to use as input for 3D printing. The nominal density of both hexagonal and square horseshoe structures is 1.23 g/cm^3.

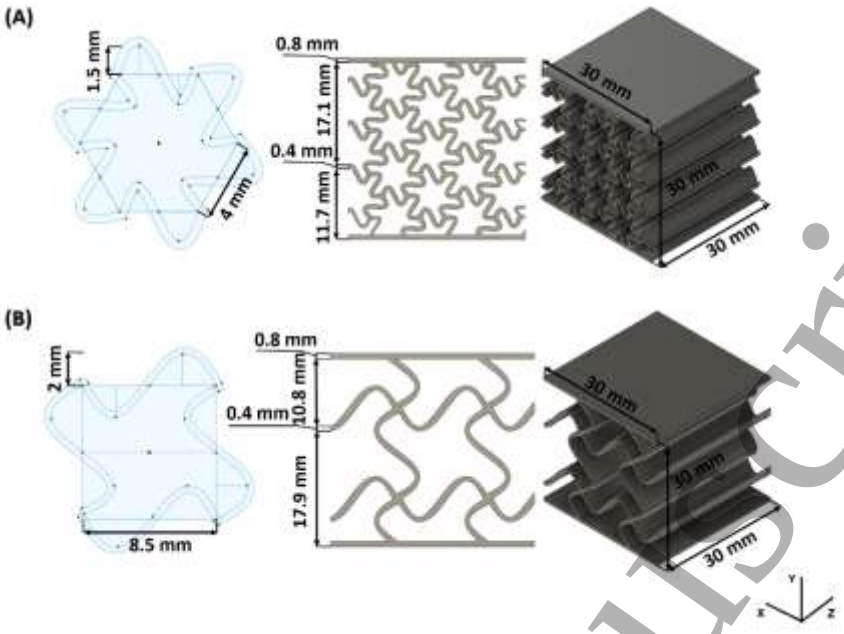

Figure 1. Design of two sandwich models; (a) Model 1: Hexagonal horseshoe shape, (b) Model 2: Square horseshoe shape.

2.3 Fabrication process and parameters

Table 2 presents the main operational parameters in the 3D printing process of the sandwich samples. The process parameters in this study are considered in the range of recommended parameters by the filament company (Ultimaker). The reference parameters in this study include a nozzle temperature of 205 °C, a print speed of 70 mm/s, and a layer height of 0.2 mm. Therefore, for investigating one specific parameter, the others were constant. In another word, 12 sets of parameters were investigated in this study.

Table 2. The operational parameters in this study

Nozzle temperature, °C	Printing speed, mm/s	Wall thickness, mm	Layer height, mm
190	50	0.4	0.1
205	70	0.5	0.2
220	90	0.6	0.3

2.4 Printing and experimental equipment

For the fabrication process, an FDM 3D printer (*Ultimaker 3 Extended, Ultimaker, The Netherlands)* with a nozzle diameter of 0.4 mm was applied and all samples are printed in XY plane. The uniaxial compression tests were conducted in the electronic universal testing machine with a maximum allowed load of 250 kN (56,202 lbf) *(Quasar 250, Galdabini, Italy)* based on ISO 7743:2017. The compression process was done to the maximum elastic limit of samples which were 10 mm (33%) for *model 1*, and 11 mm (37%) for *model 2*. The loading and unloading for the compression test were performed with a speed of 1 mm/min under displacement control mode. Additionally, unloading was also recorded to assess the mechanical response of the specimens to various printing parameters. All the experimental conditions were replicated three times at the same conditions to ensure the reliability and repeatability of the experimental results. For the

shape recovery process, all deformed samples resulted from the compression test were immersed in hot water with a temperature of 75°C (higher than the glass temperature of PLA materials) to retrieve the initial shape of the sandwich panels.

3-Finite element modeling

In the present study, a 3D finite element method by employing ABAQUS software *(V. 6.14, Dassault Systems, France)* is carried out to analyze the shape memory sandwich panels under compressive loading. Explicit dynamic analysis is employed in which simulations maintain quasi-static and lead to decreasing the simulations time providing a more efficient solution for large problems.

To model the loading-unloading cycle in the sandwich panels, an elastic-plastic model with isotropic hardening is used. In this regard, the uniaxial test data in terms of stress-strain for dog-bone specimens as well as variation of the sample's length and width measured using the digital image correlation (DIC) method are imported to ABAQUS. The DIC measurements were taken using a non-contact TRViewX high-performance extensometer (absolute accuracy ±1.5 µm). Markers were placed in the gauge area in the axial direction on the tensile samples and their displacements were recorded using the camera reflecting the axial deformation of the samples. No marker was used in the lateral direction as the camera could detect the edge of the samples in the width direction and therefore could record the variation of the width in the lateral direction. Figure 2(a) shows the dimensions of the dog-bone sample used for tensile testing and Figure 2(b) and (c) indicate the engineering stress-strain curves for the dog-bone specimens printed in horizontal and vertical directions, respectively. Values of Young's modulus, E, ultimate tensile strength (UTS) and break strain, ε_f are reported in Table 3. It can be seen that the horizontal samples show close-to-plateau (plastic) behavior after the linear region while the vertical samples show less plastic behavior. The tensile stress-strain curves and results, in terms of elongation at break, UTS, and Young's modulus compare well with other works on the similar print-orientation PLA counterparts [42, 43]. The curve with a solid line in Figure 2(b) illustrates a linear elastic behavior up to almost 1.4% (0.014) strain followed by plateau, indicating a plastic deformation growth. Because of PLA behavior, the plateau region allows for a larger amount of energy absorption at constant load; on the other hand, a smaller amount of energy is absorbed in the linear elastic deformation. Therefore the material behavior can be considered elastoplastic. As can be seen in Figure 1, thin beam-like struts are 3D printed along the printing direction and experince a dominant uniaxial stress under deformation. Theorefore, in the present study, the experimentally measured uniaxial tensile data in terms of stress-strain for horizontal samples (fabrictaed along printing direction) was implemented in the software. The FE model used in the present study is validated against the available literature data from Bodaghi et al. [37] and presented in Appendix A. As can be oserved, the FE modeling calibrated with uniaxial stress-strain data can accruratly replicate the experiment and has a close correlation with numerical method developed in [37] for lattice structures.

By creating a material calibration option in ABAQUS software and importing the DIC measured tensile properties, the elastic-plastic constants are readily determined. In doing so, the elastic modulus is determined as 3750 Mpa, and the Poisson's ratio is 0.4. Figure 3(a) shows the meshed representation of nine-cell square horseshoe shape sandwich structures. The lower jaw is entirely restricted in all directions, and the upper jaw is moved only in the vertical direction, see Figure 3(a). Furthermore, the tangential and normal behavior contact is defined between the upper jaw and the core structure and between different beam-like surfaces of the sandwich panels which would be in contact during the loading-unloading cycles. The core structure is not restricted in any direction as the contact is defined between the upper and lower jaw and core. It

is worth mentioning that for modeling loading and unloading, the upper and lower plate is considered to be rigid bodies. The references point of rigid bodies is defined so that the reaction force and displacement of the upper rigid body can be reported. Then, in the step mudulus of ABAQUS, we define two steps: loading and unloading. In the loading step, the displacement is applied to the upper plate as a boundary condition in ABAQUS load module. In the unloading step, the same as the previous step, displacement is applied in the opposite direction. After running the job, in visualization module, the force per displacement could be reported from specified references points. The amount of displacement applied in the simulation is the same as experiments i.e., 10 mm (33%) for model 1, and 11 mm (37%) for model 2.

To define the contact model in the ABAQUS, contact pressure-overclosure relationships are employed [44]. The contact stiffness (in the softened contact relationship, the contact pressure is a linear function of the clearance between the surfaces) is assumed to be high enough. Therefore, increasing contact stiffness does not significantly affect the results (load-displacement curve). It is worth mentioning that the heating-cooling process that leads to retrieving sandwich structure shape is not simulated in the present study. As in the experiment, the loading phase continues before any damage occurs in the structures, so the damage was not considered in the finite element analysis

Linear hexahedron elements, type C3D8R, are used to mesh the sandwich structures, and linear quadrilateral elements, type R3D4, are employed to mesh the upper and lower jaw. In addition, the mesh refinement technique is done by decreasing the size of elements, so increasing the number of elements until the load-displacement curves converge. For example, for model 2 (0.4 mm thicknesses) as indicated in Figure 3(b), as the number of meshes is increased to 11500 meshes, the load-displacement curve converges to the same value, so the number of meshes for model 2 is more than 11500 elements. Mesh analysis is done for all the samples with different cell numbers and thicknesses.

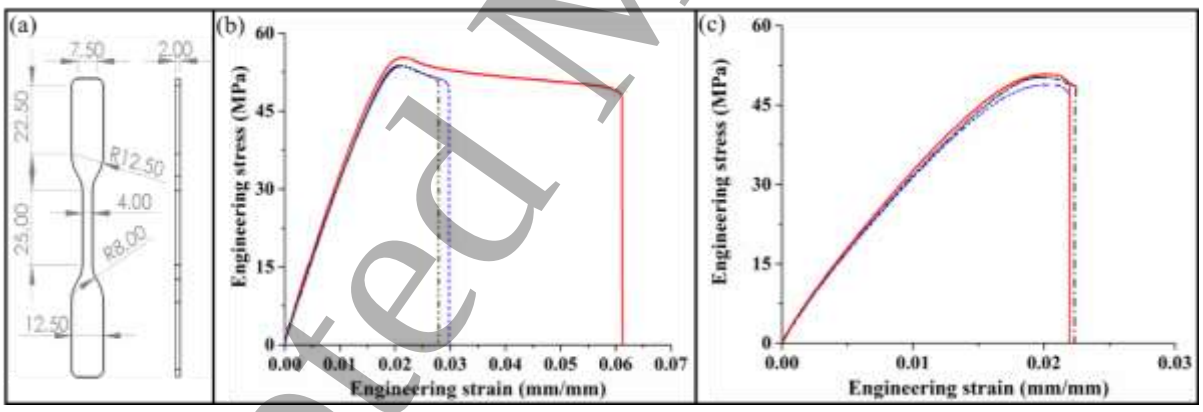

Figure 2 (a) Dimensions of the tensile sample according to ISO 37:2017 standard, (b) and (c) Experimentally measured uniaxial tensile data in terms of stress-strain for horizontal and vertical samples on the build plate, respectively.

Table 3. Mechanical properties of the printed specimens determined from the standard tensile tests

Specimen type/direction	E (GPa)	σ_U (UTS) (MPa)	ε_f (%)
Horizontal	3.49 ± 0.18	54.18 ± 0.66	3.6 ± 1.45
Vertical	4.06 ± 0.17	49.5 ± 0.68	2.21 ± 0.02

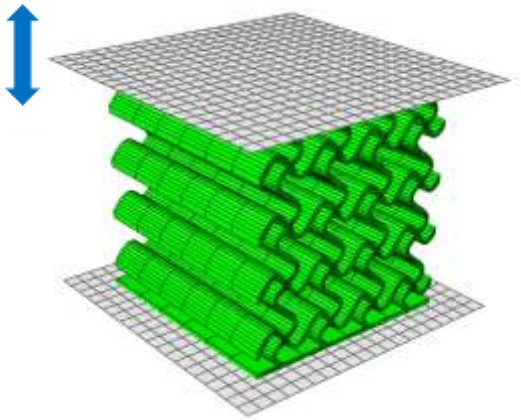

(a)

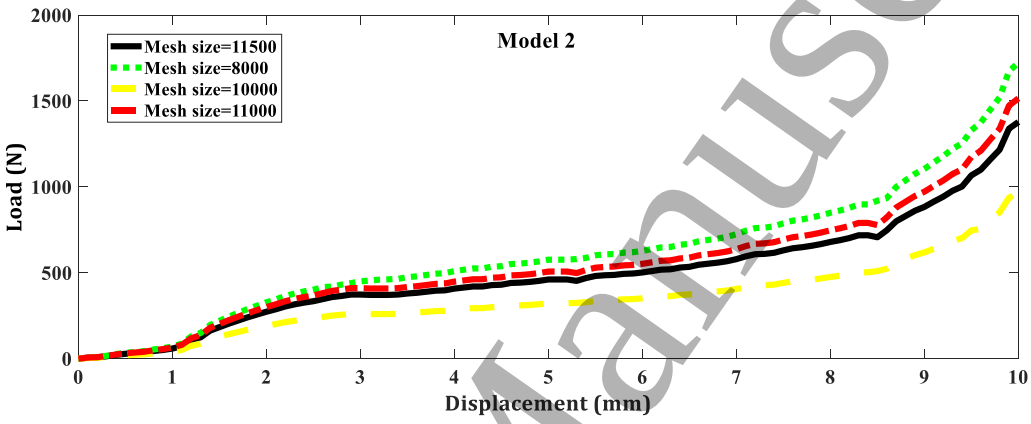

(b)

Figure 3 (a) The meshed presentation of a nine-cell sandwich panel (nine-cell model 2), (b) mesh sensitivity analysis for model 2

4-Results and discussion

4.1 Experimental vs. simulation results

In this section, the deformation of sandwich structures under loading-unloading conditions are investigated experimentally and numerically for models 1 and 2. Compression tests on the printed structures were conducted to extract the loading/unloading force-displacement graphs and simulations were performed in ABAQUS compressing the structure under the same conditions as experiments. The geometric dimensions of the FE model are the same as the samples presented in Figure 1. Figures 4 and 5, parts (a)-(c) and (e)-(g) show shapes of the sandwich panels under loading-unloading cycle obtained from experiments and simulations, for models 1 and 2, respectively, while part (d) depicts the configuration after heating then cooling down to the room temperature which is obtained by experiment. Part (h) also compares load-displacement curves from experiments and FEM. Part (i) illustrates dissipated energy and absorbed energy by the sandwich panel, which is determined based on load-displacement experimental data. By comparing experimental and numerical results in Figures 4 and 5, it is perceived that the numerical modeling using ABAQUS software employing elastic-plastic model in which the constants are determined based on stress-strain curve determined by the experimental test is reliable. There is a good agreement between the FEM results and experimental tests under a large deformation for both models 1 and 2. It should be noted that there is an insignificant difference between FEM modeling and experimental study, which is

associated with geometrical imperfection in the 3D printed samples and simplifications of the modeling.

One of the fundamental parameters for analyzing the energy absorption of sandwich structures is specific energy absorption (SEA) which is defined as the unit energy absorption efficiency of the sandwich beams, written as :

$$SEA = \frac{Absorbed\ Energy}{Mass} \quad (1)$$

In model 1 (Figure 4), related to hexagonal horseshoe shape sandwich panel, by applying a compressive load, the beam-like members are rotated and also deformed to withstand the compressive load without fracture. Indeed these beam-like members undergo local buckling. After the unloading stage, this panel remained deformed, which means structures experienced plastic deformation. Figure 4(h) shows that at the initial stage of applying compressive displacement (until stroke 3mm) the compressive load increases by a steep slope in the elastic deformation range. Afterward, at the approximately constant compressive loading, the structure undergoes a large deformation in the plastic deformation range. At stroke 7mm, the beam-like members' surfaces contact with each other, and the overall stiffness of structures increases due to becoming dense solid form structures, and the compressive load is increased significantly.

As illustrated in Figure 4(h), the difference between the maximum compressive load in the experimental study and the one predicted by numerical modeling is not significant. At the unloading stage, the panel tends to recover to the initial shape. However, some plastic strains remain in the sandwich panel, so the structure recovers partially. The FEM analysis also illustrates the deformation after unloading with good accuracy. When this structure is heated, this residual plastic strain is released and it transforms to its initial form after cooling, see Figure 4(d). The reversibility of the sandwich panel, in which residual plastic strain is released by heating, is indicated by a red dash line in Figure 4(h).

Figure 4(i) shows the energy graph of the hexagonal horseshoe shape structure, which is highlighted by the area under the load-displacement curve. The energy applied to the structure by compressive loading is divided into two parts: kinetic energy of deformation of the structure at the unloading stage and dissipated due to the residual plastic strain. The amount of energy dissipated (red area) and absorbed energy (green area) are 3.730 J and 0.670 J, respectively. In addition, according to Eq. (1), SEA is 0.065 J/gr.

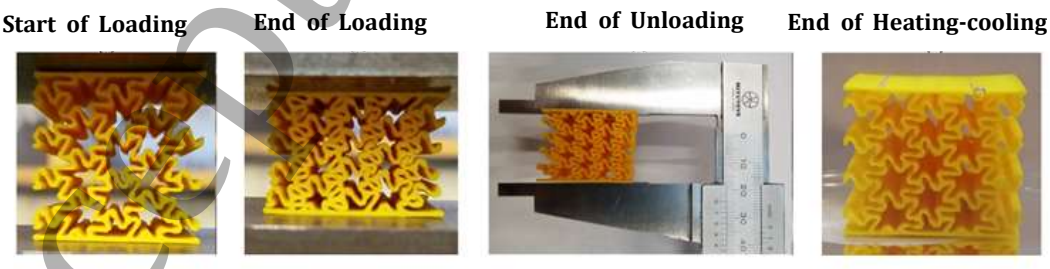

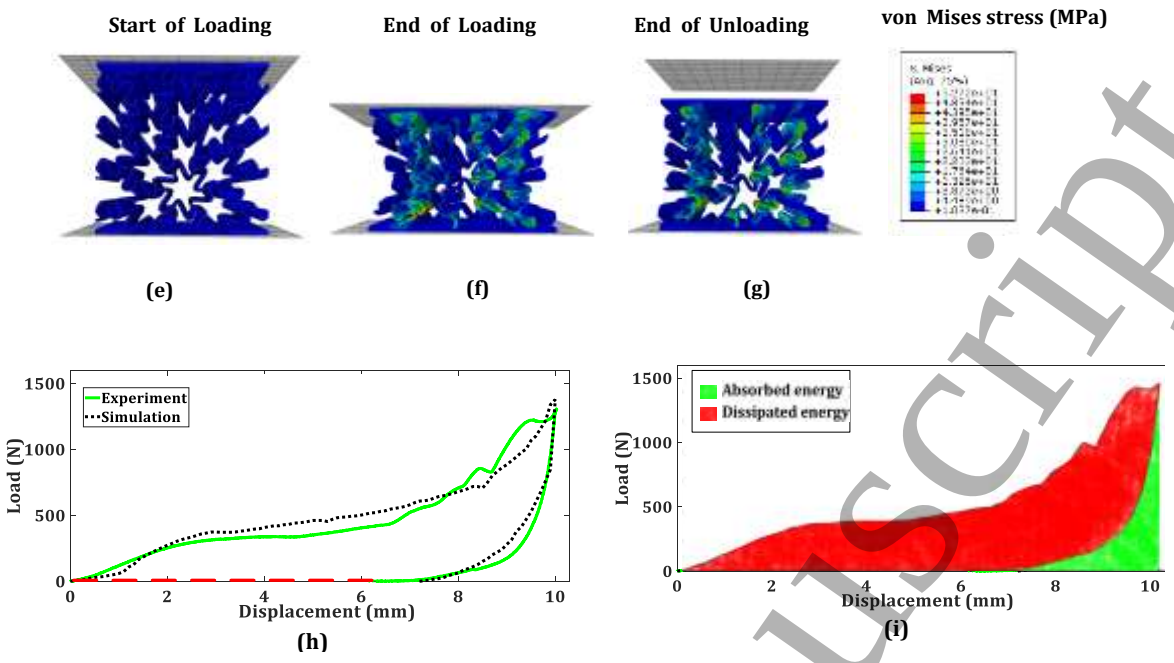

Figure 4. Sandwich structure, model 1 (a-g) experimental and simulation shape, (h) load-displacement curve for loading-unloading and thermal shape recovery (plastic strain recovery by thermal stimuli is indicated by the red dash line), (i) dissipated and absorbed energies by the sandwich panel.

Figure 5 shows the deformation configuration and mechanical response of model 2, square horseshoe shape, under loading-unloading conditions. By comparing Figure 5(a-c) and Figure 5(e-g), it is found that the numerical FEM analysis shows a deformation configuration close to the experimental study. Even the numerical analysis is capable of modeling the unloading configuration with reasonable accuracy, which shows that the elastic-plastic model is reliable for predicting the deformation of 3D printing shape-memory sandwich panels. It is worth mentioning that the difference between experiments and present simulations could be due to geometrical imperfection in the 3D printed samples and some assumptions to simplify the model used, such as contact properties between jaw and sample and between different parts of structures. Also, using the elastic-plastic model to simulate the structure is reliable, and the best choice is selected based on several iterations, comparing numerical and experimental results.

The stress contour is shown in Figure 5, which indicates that the maximum von Mises stress happens in the curved beam-like members, and this area is susceptible to failure. The numerical and experimental observation reveals that deformations usually start from the top of the specimen that is close to the upper jaw. In these structures, the deformation has a wave-like form that starts at the top of the sandwich structure and propagates until it reaches the bottom of the structure. Then, most beam-like surfaces contact, and the sandwich panel becomes denser than the initial form.

Figure 5(h) indicates the load-displacement curve for model 2, both numerical FEM analysis and experimental test. As seen in this figure, the numerical FEM modeling based on the elastic-plastic model predicts the load-displacement curve close to the experimental test. The load-displacement curve shows an initial softening, in which the load increases by small deformation due to the auxetic behavior in the elastic deformation regime. Between stroke 3-4 mm, at a constant load, the deformation increases. At stroke 4 mm, the structures lose their stability and

experience a softening snap-through type of buckling in which structures under specified loading are transformed from an equilibrium state to an unstable condition. In this stage, the structure undergoes a significant geometric change. At the end of the loading stage, the structures become denser, and due to the interaction of beam-like surfaces, the structure experiences significant hardening and increasing loading. At stroke 11mm, the unloading stage happens, and structures want to recover to the initial form, although because of residual plastic strain, this does not happen entirely. When the heating-cooling process is done, and the structure transforms to its initial form, see Figure 5(d). The residual plastic strain relief is indicated by the red dash line in Figure 5(h).

Figure 5(i) shows the energy distribution graph of square horseshoe shape sandwich panels. The total energy distributed is calculated as 1.2 J with 0.995 J (red area) accounting for dissipation and 0.205 J (green area) for absorption energy; also, according to Eq. (1), SEA is 0.043 J/gr. By comparing models 1 and 2, it should be noted that the energy absorption of model 1 is 3 times higher than model 2. One of the main reasons is that the inner density of the core in Model 1 is higher than in model 2. In addition, the SEA of Model 1 is increased by 51% compared to model 2. Therefore, increasing the inner density leads to increasing the energy absorption, the mass of structures is increased too. So the SEA of model 1 is not rising as energy absorption.

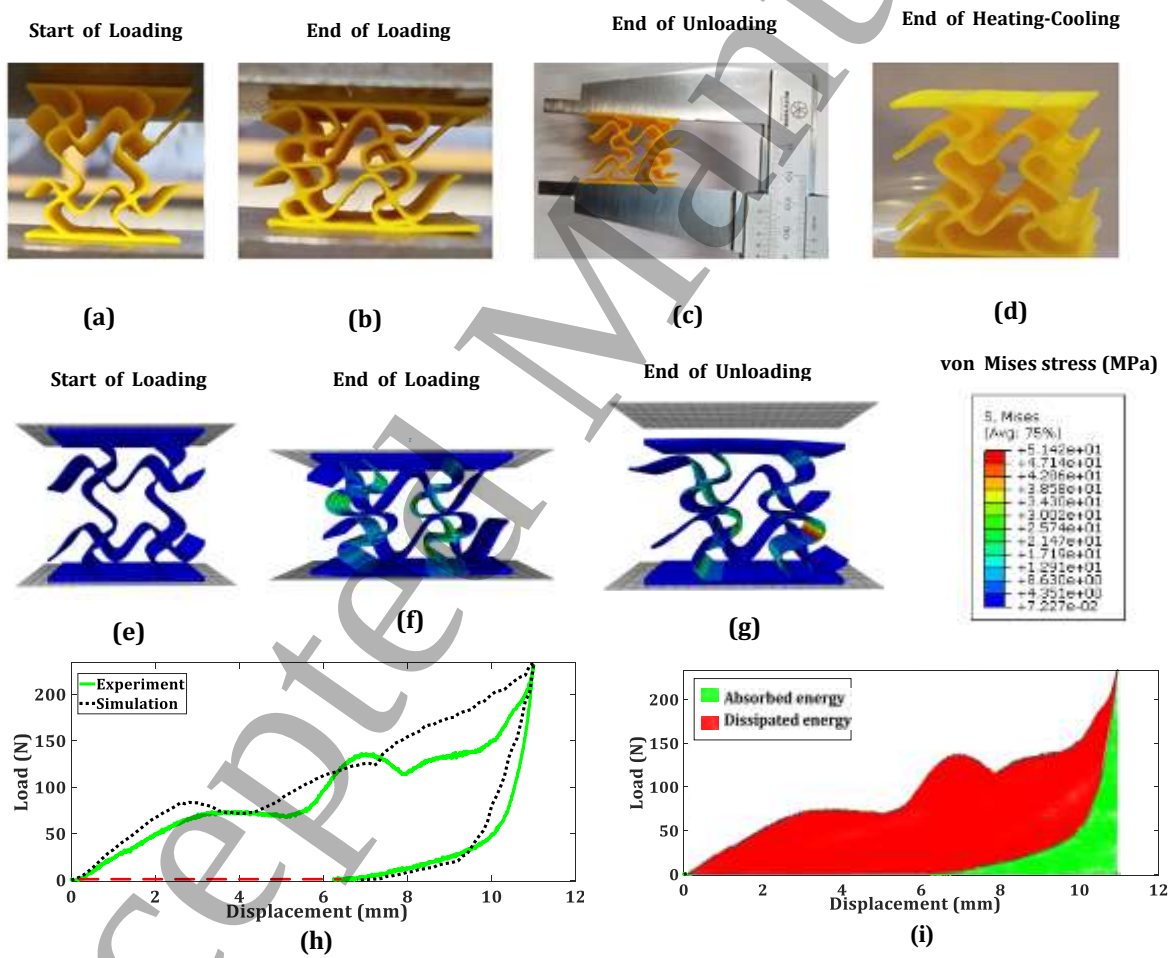

Figure 5. Sandwich structure, model 2 (a-g) experimental and simulation shape, (h) load-displacement curve for loading-unloading and thermal shape recovery (plastic strain recovery by thermal stimuli is indicated by the red dash line), (i) dissipated and absorbed energies by the sandwich panel.

This study also investigates the impact of design, particularly the inner core quantity of inner density, on the functionality of the sandwich structure. Figure 6 (a-d) exemplifies numerically and experimentally the results of the compression test for four groups of specimens (for model 2), including one, four, nine, and sixteen cells, respectively. In general, the load considerably increases by adding more cells while maximum displacement decreases at the same time. For example, obviously, by increasing the cells from one to four, the mechanical force sharply increases (almost double), and in opposite the maximum deformation is reduced by 2 mm. Further increasing cell count to 9, it is observed that deformation is even less at 8 mm, but the load increases up to 0.6 kN compared with 0.2 kN for one cell. The highest load was achieved by 16 cell structures with a load of 1.6 kN, but maximum deformation of 7 mm.

As seen in Figure 6, FEM modeling predicts the load-displacement curve with good accuracy. The numerical modeling shows the same trend as the experimental study, in which by increasing the numbers of cells, the maximum load increases and the displacement decreases. It is seen that by increasing the cell numbers or inner density, the shape memory sandwich panel shows an initial hardening, and the compressive load increases dramatically, especially for four and nine cells, which is due to increasing numbers of beam-link members, which deformed and experienced local bending and buckling. Indeed, geometrical non-linearity, densification, and plastic deformation result in the hardening of the sandwich panel during the loading.

As it is seen, by increasing the cell number, some fluctuations occur in the structures successively (for four and nine cells) that is because of collapses of beams during deformation, which results in a softening behavior. Such softening–hardening responses in the compressive loading is related to the snap-through of beam-like buckling of the members, which increases by increasing the cell numbers. The results also show that energy absorbed by the sandwich panel with 1 cell is 0.205 J while the energy absorbed by sandwich structures with 16 cells is almost 0.832 J which is 4 times higher than the 1 cell sandwich panel. In this regard, increasing cell numbers has a significant impact on energy absorption.

The SEA for the sandwich panel (model 2) with 1 cell and model 1 with 16 cells are 0.043 J/gr and 0.071 J/gr, respectively. Therefore SEA is increased by 65%, which is significant. The reason is that the structure with 16 cells is denser and needs more force to compress and, as a result, absorb more energy. It is worth mentioning that the weight of structures is also increased by increasing the number of cells, but the increasing rate of energy absorbed is higher than the increased rate of the weight, so the SEA increased by increasing the number of cells.

This behavior can be useful in variable stress absorption applications. For example, if the goal is to absorb impacts with the exact dimensions and high load capabilities, there will be no need to change the design of the smart sandwich structure. Instead, the remedy is the multiplication of the same design with a higher density inside the core. In 3D printing applications, this method has the potential to save valuable research time and to have predictable results.

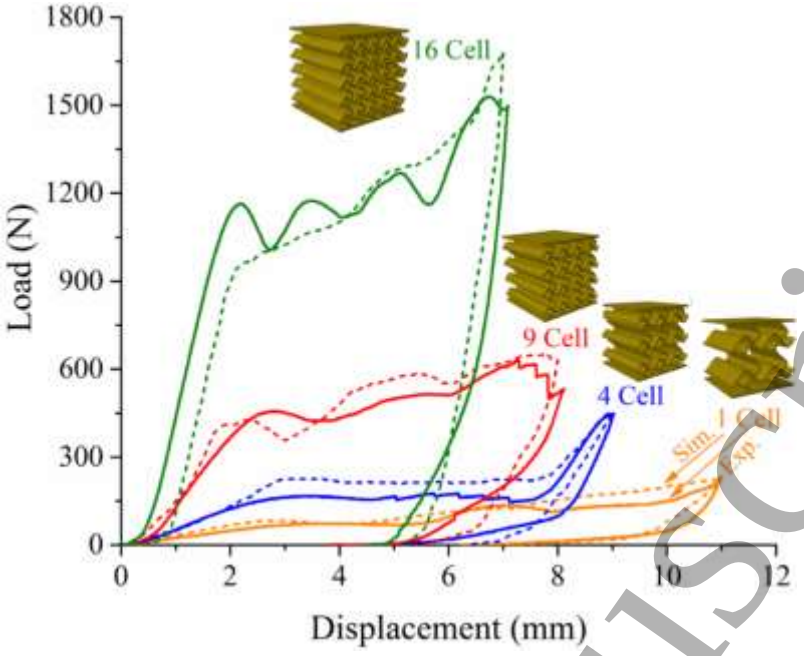

Figure 6. The impact of cell quantity on the functionality of sandwich structures (model 2), comparison between simulations (Sin.) and experiments (Exp.)

Wall thickness is another parameter investigated numerically and experimentally for both models, without the change of internal structure or any printing parameters. Figure 7 (a-c) shows the load-displacement curve for different wall thicknesses for model 1, in which the maximum applied displacement (for both FEM and experiment) is 10 mm, and Figure 7 (d-f) shows the load-displacement curve for different wall thicknesses for model 2 in which the maximum applied displacement (for both FEM and experiment) is 11 mm. As can be seen, increasing the wall thickness has a direct impact on the loading force so that, as shown for model 1, the load rate rises from 1.2 kN to 2.2 kN when the sample thickness increases from 0.4 mm to 0.6 mm. Model 2 also has a similar trend, and the load rate grows up from 0.2 kN to 0.5 kN when the wall thickness of the sample increases from 0.4 mm to 0.6 mm. Both experimental and numerical results reveal that this variation is very successful in increasing load without losing maximum deformation. Similar to internal cell count, this method can be quickly adapted for specific stress absorption tasks without changing any external dimensions. In contrast to inner cell count, this variation has a lower load increasing scale, making it more accurate and yields more predictable results.

The energy absorbed by sample 1 with 0.4 mm wall is 0.670 J, and for sample 1 with 0.6 mm wall thickness is 0.852 J, that reveals by increasing the wall thickness from 0.4 mm to 0.6 mm, the absorbed energy is increased almost by 27%. In addition, this amount for sample 2 with 0.4 mm thickness and 0.6 mm thickness are 0.205 J and 0.395 J, respectively. Therefore, increasing the wall thickness from 0.4 mm to 0.6 mm results in increasing energy absorption by 93%. The SEA for model 1 with 0.4 mm wall is 0.065 J/gr, and for model 1 with 0.6 mm wall thickness is 0.069 J/gr which is increased by 6.2%. SEA for Model 2 with 0.4 mm thickness and 0.6 mm thickness are 0.043 J/gr and 0.062 J/gr, respectively, so SEA is increased by 44.2%, which is significant.

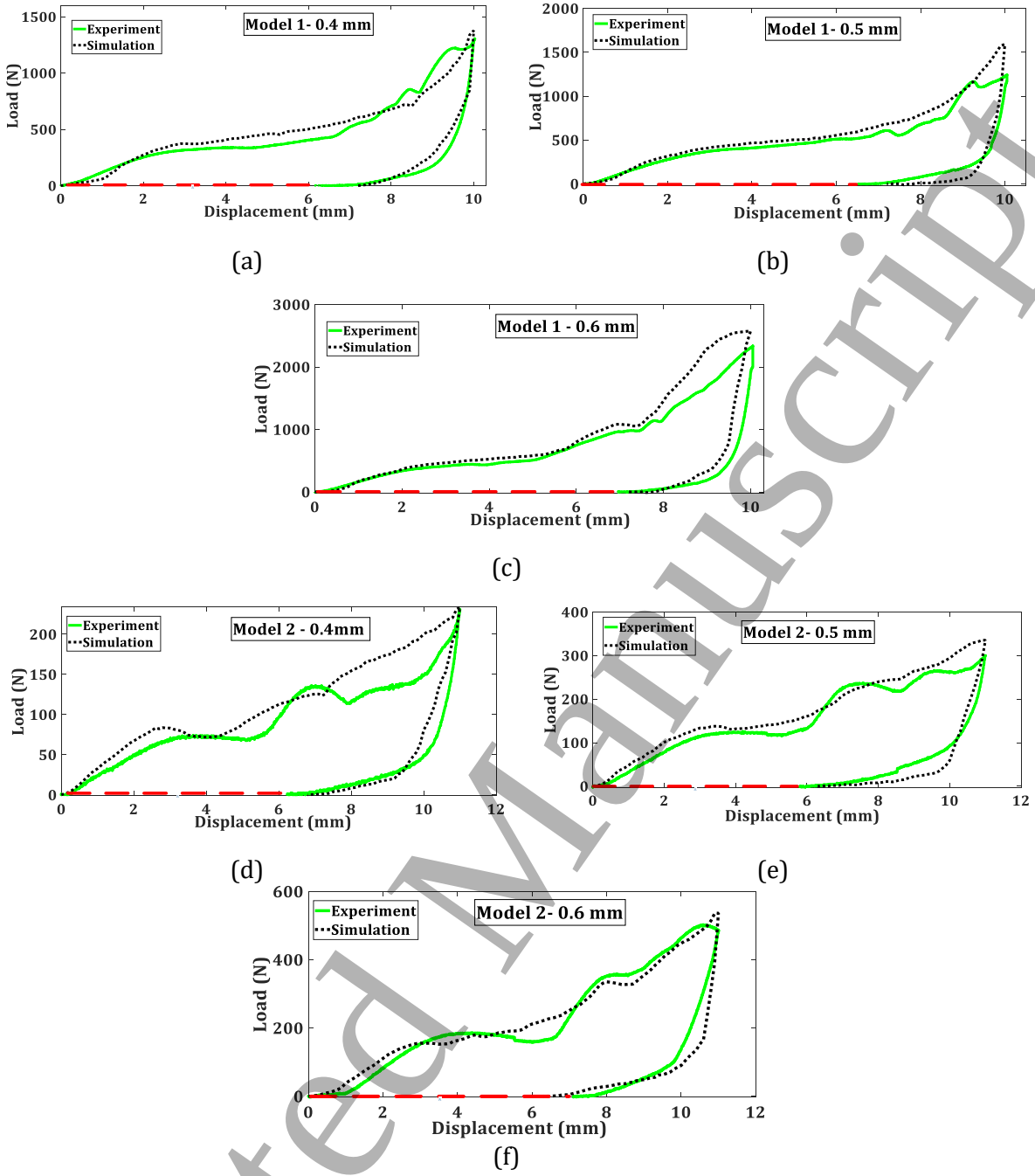

Figure 7. The influence of wall thickness on stress absorption rate; (a-c) model 1, (d-f) model 2

4.2 Influence of processing parameters

Various studies show the impact of operational parameters on the functionality of 4D printed structures [45]. This study also investigates the influence of printing parameters, including layer height, nozzle temperature, and printing speed, on the compression strength of the fabricated samples. As shown in Figure 8, the compressive load reduces by increasing layer height from 0.1 mm to 0.3 mm for both models. Nozzle temperature shows an opposite trend so that the compressive load increases considerably by raising the nozzle temperature from 190 °C to 220 °C. However, it seems varying printing speed does not influence compressive load in a linear pattern, and overall does not influence the load significantly. Instead, a slower print speed of 50

mm/s results in more even compression behavior compared with a higher print speed of 90 mm/s for both samples.

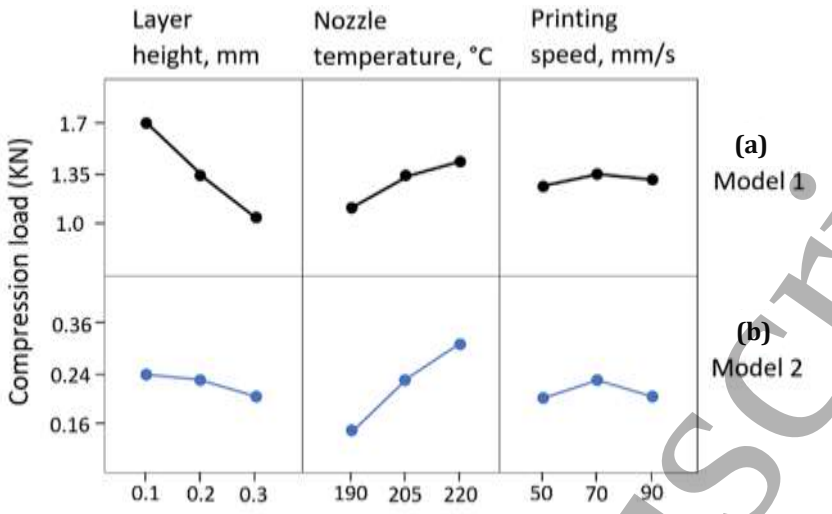

Figure 8. The influence of printing parameters, including layer height, nozzle temperature, and printing speed, on the mechanical strength of printed samples; (a) model 1, (b) model 2

5-Conclusions

This research work provided advancement to understand the functionality of 4D printed smart sandwich structures for reversible energy absorption applications. For this purpose, two different geometrical sandwich structures, hexagonal and square horseshoe shapes, were designed and fabricated by the FDM printing approach using shape memory PLAs. The impact of design, particularly core shape and quantity, and printing parameters, namely layer height, nozzle temperature, and printing speed, on the functionality of fabricated samples were investigated. Also, numerical modeling using the finite element method was applied in this study in order to predict the mechanical behavior of the structures in the compression test.

The experiment results revealed that the highest impact on energy absorption rate is from increased internal cell count; however, it significantly sacrifices the maximum deformation compared with standard samples. Therefore, finding the optimal processing parameters is vital to prevent any changes in the maximum deformation depth of the sandwich structure. A comparison between the simulation and experimental results revealed that the developed prediction model is a reliable tool in order to evaluate the mechanical behavior of the sandwich panels under the external loading-unloading process. The material-structural model, designs, and results provided in this paper are expected to be instrumental towards 4D printing tunable meta-structures for reversible energy absorption applications such as crashworthiness applications or personal protective equipment (PPE) to minimize hazards that could make serious injuries. This study could be applied as a useful source for designers to tailor the sandwich structures based on their needs for creating the final product.

6-References

1. Zhou, Y., et al., *From 3D to 4D printing: approaches and typical applications.* Journal of Mechanical Science and Technology, 2015. **29**(10): p. 4281-4288.
2. Hu, W., et al., *Deformation behavior and band gap switching function of 4D printed multi-stable metamaterials.* Materials & Design, 2021. **200**: p. 109481.

3. Kuang, X., et al., *Advances in 4D printing: materials and applications.* Advanced Functional Materials, 2019. **29**(2): p. 1805290.
4. Bodaghi, M. and W. Liao, *4D printed tunable mechanical metamaterials with shape memory operations.* Smart Materials and Structures, 2019. **28**(4): p. 045019.
5. Scalet, G. *Two-way and multiple-way shape memory polymers for soft robotics: An overview*. in *Actuators*. 2020. Multidisciplinary Digital Publishing Institute.
6. Ji, L., et al., *Compression behavior of the 4D printed reentrant honeycomb: experiment and finite element analysis.* Smart Materials and Structures, 2020. **29**(11): p. 115016.
7. Hu, G., et al., *Increasing dimension of structures by 4D printing shape memory polymers via fused deposition modeling.* Smart Materials and Structures, 2017. **26**(12): p. 125023.
8. Kačergis, L., R. Mitkus, and M. Sinapius, *Influence of fused deposition modeling process parameters on the transformation of 4D printed morphing structures.* Smart Materials and Structures, 2019. **28**(10): p. 105042.
9. Teoh, J.E.M., et al., *Multi-stage responsive 4D printed smart structure through varying geometric thickness of shape memory polymer.* Smart Materials and Structures, 2017. **26**(12): p. 125001.
10. Mehrpouya, M., et al., *Investigation on the Functionality of Thermoresponsive Origami Structures.* Advanced Engineering Materials, 2020. **22**(8): p. 2000296.
11. Dogan, S., et al., *Thermally induced shape memory behavior, enzymatic degradation and biocompatibility of PLA/TPU blends:"Effects of compatibilization".* Journal of the mechanical behavior of biomedical materials, 2017. **71**: p. 349-361.
12. Ze, Q., et al., *Magnetic shape memory polymers with integrated multifunctional shape manipulation.* Advanced Materials, 2020. **32**(4): p. 1906657.
13. Renata, C., et al., *Shape change/memory actuators based on shape memory materials.* Journal of Mechanical Science and Technology, 2017. **31**(10): p. 4863-4873.
14. Sarvestani, H.Y., et al., *3D printed meta-sandwich structures: Failure mechanism, energy absorption and multi-hit capability.* Materials & Design, 2018. **160**: p. 179-193.
15. Wagner, M.A., et al., *Programmable, active lattice structures: Unifying stretch-dominated and bending-dominated topologies.* Extreme Mechanics Letters, 2019. **29**: p. 100461.
16. Ge, L., et al., *Compression behavior of a novel sandwich structure with bi-directional corrugated core.* Thin-Walled Structures, 2021. **161**: p. 107413.
17. Wu, W., et al., *Mechanical design and multifunctional applications of chiral mechanical metamaterials: A review.* Materials & Design, 2019. **180**: p. 107950.
18. Safarabadi, M., et al., *Experimental and numerical study of buckling behavior of foam-filled honeycomb core sandwich panels considering viscoelastic effects.* Journal of Sandwich Structures & Materials, 2021. **23**(8): p. 3985-4015.
19. Qi, J., et al., *Energy absorption characteristics of origami-inspired honeycomb sandwich structures under low-velocity impact loading.* Materials & Design, 2021. **207**: p. 109837.
20. Xin, X., et al., *Origami-inspired self-deployment 4D printed honeycomb sandwich structure with large shape transformation.* Smart Materials and Structures, 2020. **29**(6): p. 065015.
21. Jian, B., et al., *Origami-based design for 4D printing of 3D support-free hollow structures.* Engineering, 2022.
22. Peng, C., et al., *3D printed sandwich beams with bioinspired cores: Mechanical performance and modelling.* Thin-Walled Structures, 2021. **161**: p. 107471.
23. Kueh, A. and Y. Siaw, *Impact resistance of bio-inspired sandwich beam with side-arched and honeycomb dual-core.* Composite Structures, 2021. **275**: p. 114439.
24. Askari, M., et al., *Additive manufacturing of metamaterials: A review.* Additive Manufacturing, 2020: p. 101562.
25. Bertoldi, K., et al., *Flexible mechanical metamaterials.* Nature Reviews Materials, 2017. **2**(11): p. 1-11.

26. Chen, D. and X. Zheng, *Multi-material additive manufacturing of metamaterials with giant, tailorable negative Poisson's ratios.* Scientific reports, 2018. **8**(1): p. 1-8.
27. Lv, W., D. Li, and L. Dong, *Study on blast resistance of a composite sandwich panel with isotropic foam core with negative Poisson's ratio.* International Journal of Mechanical Sciences, 2021. **191**: p. 106105.
28. Shao, Y., et al., *Insight into the negative Poisson's ratio effect of the gradient auxetic reentrant honeycombs.* Composite Structures, 2021. **274**: p. 114366.
29. Zamani, M.H., M. Heidari-Rarani, and K. Torabi, *Optimal design of a novel graded auxetic honeycomb core for sandwich beams under bending using digital image correlation (DIC).* Composite Structures, 2022: p. 115310.
30. Zamani, M.H., M. Heidari-Rarani, and K. Torabi, *A novel graded auxetic honeycomb core model for sandwich structures with increasing natural frequencies.* Journal of Sandwich Structures & Materials, 2021: p. 10996362211030565.
31. Rahman, H., et al., *Energy absorption and mechanical performance of functionally graded soft–hard lattice structures.* Materials, 2021. **14**(6): p. 1366.
32. Townsend, S., et al., *3D printed origami honeycombs with tailored out-of-plane energy absorption behavior.* Materials & Design, 2020. **195**: p. 108930.
33. Jiang, Y. and Y. Li, *3D printed auxetic mechanical metamaterial with chiral cells and re-entrant cores.* Scientific reports, 2018. **8**(1): p. 1-11.
34. Liu, K., et al., *4D printed zero Poisson's ratio metamaterial with switching function of mechanical and vibration isolation performance.* Materials & Design, 2020. **196**: p. 109153.
35. Bates, S.R., I.R. Farrow, and R.S. Trask, *3D printed polyurethane honeycombs for repeated tailored energy absorption.* Materials & Design, 2016. **112**: p. 172-183.
36. Mehrpouya, M., et al., *Investigation on shape recovery of 3D printed honeycomb sandwich structure.* Polymers for Advanced Technologies, 2020. **31**(12): p. 3361-3365.
37. Bodaghi, M., et al., *Reversible energy absorbing meta-sandwiches by FDM 4D printing.* International Journal of Mechanical Sciences, 2020. **173**: p. 105451.
38. Barletta, M., A. Gisario, and M. Mehrpouya, *4D printing of shape memory polylactic acid (PLA) components: Investigating the role of the operational parameters in fused deposition modelling (FDM).* Journal of Manufacturing Processes, 2021. **61**: p. 473-480.
39. Zeng, C., et al., *Temperature-dependent mechanical response of 4D printed composite lattice structures reinforced by continuous fiber.* Composite Structures, 2022. **280**: p. 114952.
40. Liu, T., et al., *4D printed anisotropic structures with tailored mechanical behaviors and shape memory effects.* Composites Science and Technology, 2020. **186**: p. 107935.
41. Yang, X., et al., *Out-of-plane crashworthiness analysis of bio-inspired aluminum honeycomb patterned with horseshoe mesostructure.* Thin-Walled Structures, 2018. **125**: p. 1-11.
42. Letcher, T. and M. Waytashek. *Material property testing of 3D-printed specimen in PLA on an entry-level 3D printer*. in *ASME International Mechanical Engineering Congress and Exposition*. 2014. American Society of Mechanical Engineers.
43. Kumar, S.A. and Y.S. Narayan, *Tensile testing and evaluation of 3D-printed PLA specimens as per ASTM D638 type IV standard*, in *Innovative Design, Analysis and Development Practices in Aerospace and Automotive Engineering (I-DAD 2018)*. 2019, Springer. p. 79-95.
44. Abaqus, F., *Dassault Systemes Simulia Corporation.* Providence, Rhode Island, USA, 2014.
45. Heidari-Rarani, M., et al., *Optimization of FDM process parameters for tensile properties of polylactic acid specimens using Taguchi design of experiment method.* Journal of Thermoplastic Composite Materials. **0**(0): p. 0892705720964560.

Appendix A. Validation of proposed FE model with available literature data

In order to validate the proposed FE model, the structure simulated by Bodaghi et al. [37] is simulated by the model used in the present study. Bodaghi et al. [37] applied compressive

mechanical load to the SMP meta-structure and investigated the reversibility of this structure. The reason for considering this study for validation is that they consider elastic-plastic bahevior of modeling SMP with unloading condition. The results are presented in Figure A1.

Figure A1(a-c) indicates different structure shapes under the loading-unloading cycle, proving that the proposed model in the present study can predict the deformation of structures closely similar to Bodaghi et al.'s work. Figure A1(d) shows the force-displacement curve for the present model and available results, which shows that the present model predicts force-displacement with good accuracy.

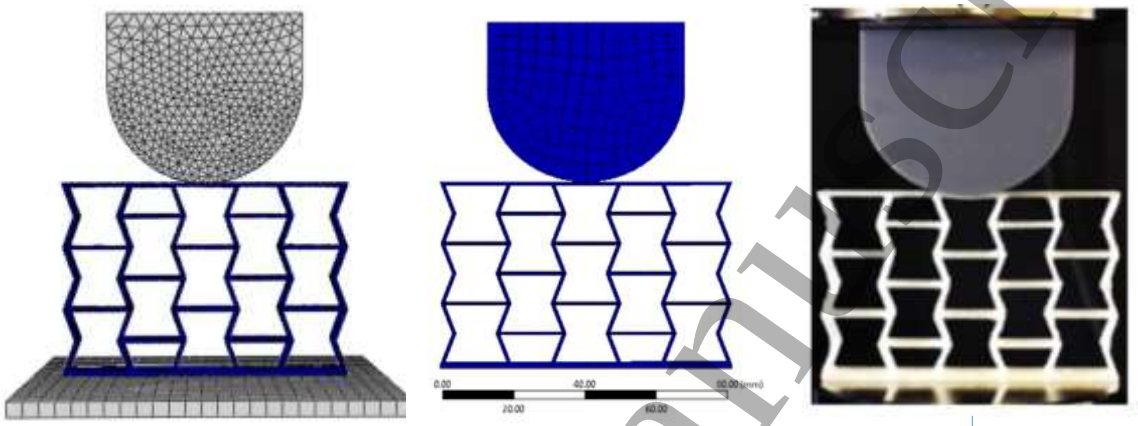

(a) Start of loading

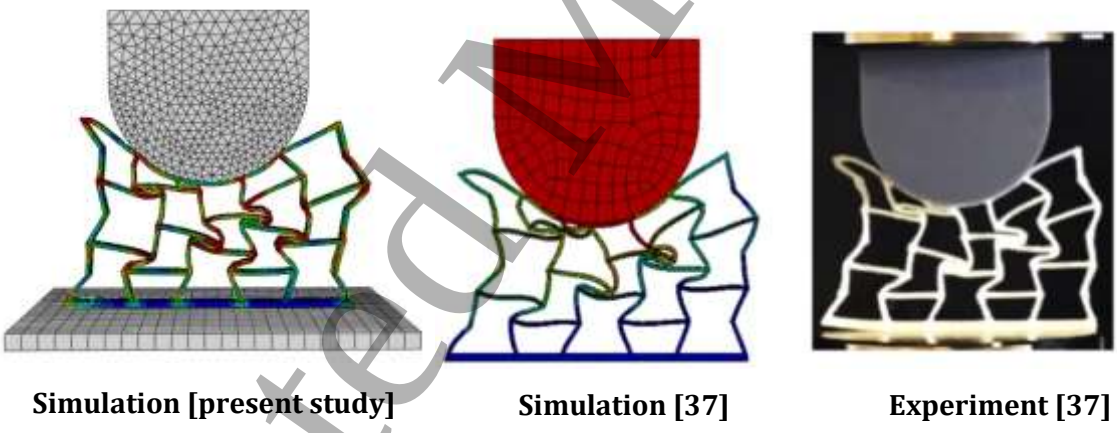

(b) End of loading

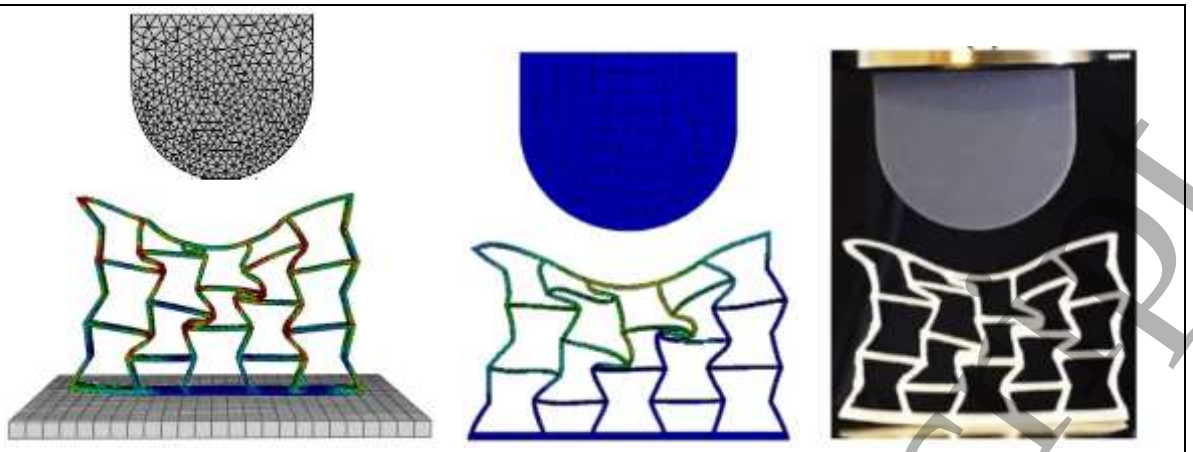

(c) End of unloading

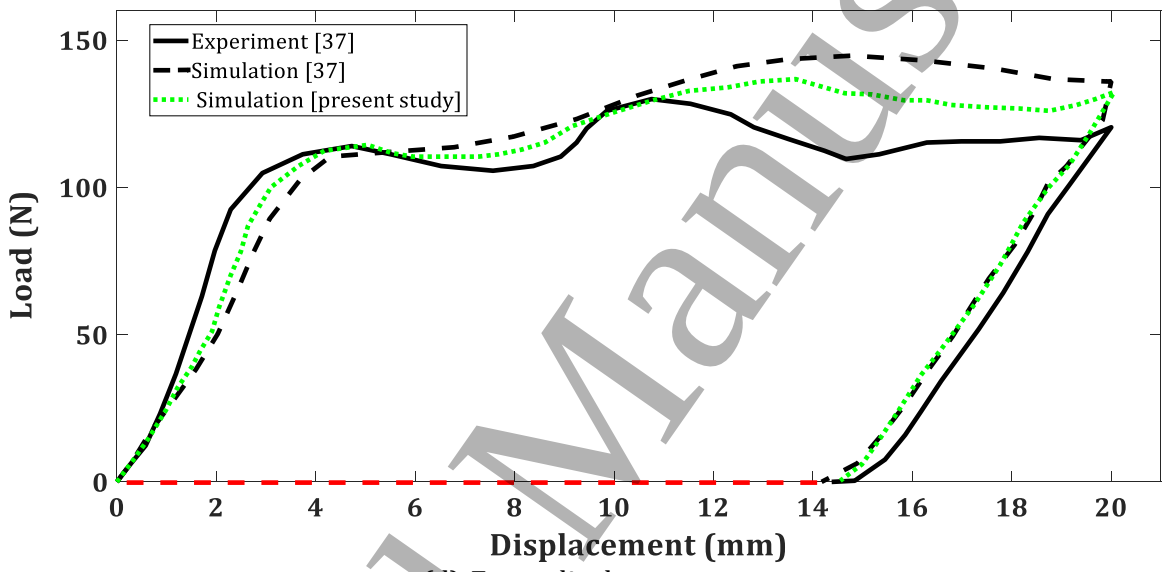

(d) Force-displacement curve

Figure A1 Validation of the proposed model in the present study with available literature results [37] in different stages: (a) Start of loading, (b) End of loading, (c) End of unloading, and (d) force-displacement curve